Mechanics of Advanced Composite Structures 9 (2022) 75 – 88

Semnan University

Mechanics of Advanced Composite Structures

journal homepage: https://MACS.journals.semnan.ac.ir

Buckling and Nonlinear Vibration of Functionally Graded Porous Micro-beam Resting on Elastic Foundation

V. H. Dang *, T. H. Nguyen

Department of Mechanics, Thai Nguyen University of Technology, Thainguyen, Vietnam

KEYWORDS

Micro-beams;
Nonlocal strain gradient theory;
Functionally graded porous;
Buckling;
Nonlinear vibration.

ABSTRACT

The buckling and nonlinear free vibration problems of functionally graded porous (FGP) micro-beam resting on an elastic foundation are presented through the nonlocal strain gradient theory (NSGT) and the Euler-Bernoulli beam theory (EBT) with the von-Kármán's geometrical nonlinearity. The micro-beam is made up of metal and ceramic in which the material properties are assumed to be varied continuously in the thickness direction through a simple exponential law. Two porosity distribution models, including even and uneven distributions, are considered. The governing equation of motion is derived by employing Hamilton's principle. The analytical expressions of the critical buckling force and nonlinear frequency of the FGP micro-beam with simply supported (S-S) boundary conditions (BCs) are obtained by utilizing the Galerkin technique and the equivalent linearization method (ELM). The reliability of the obtained results has been checked. Effects of the power-law index, the porosity distribution factor, the length-thickness ratio, the material length scale parameter (MLSP), the nonlocal parameter (NP), and the coefficients of the elastic foundation on the buckling and nonlinear free vibration responses of the FGP micro-beam are investigated and discussed in this work.

1. Introduction

By combining materials into a uniform volume, functionally graded (FG) materials showed prominent advantages compared with the traditional composite materials. Nowadays, FG materials are widely used in many fields, especially in aerospace engineering, nuclear engineering, biomedical engineering, and optical engineering [1-3]. Fallah and Aghdam [4] investigated the post-buckling and nonlinear free vibration behaviors of FG beams on nonlinear elastic foundations. Using various higher-order shear deformation beam theories, Thai and Vo [5] presented the analysis of the linear free vibration and bending responses of FG beams. The multi-scale method was applied by Yan et al. [6] to study the stability of an axially moving FG beam with time-dependent velocity. In manufacturing FG materials, it is difficult to avoid the appearance of micro-voids or pores inside the FG materials. The existence of pores reduces the weight but increases the ability to absorb the energy of FG materials [7, 8]. Therefore, the influence of porosity on the mechanical behavior of FG structures needs to be studied in detail. Wattanasakulpong and Chaikittiratana [9] first studied the influence of porosity on the vibration behavior of beams. In this work, the authors introduced two models of porosity distribution in FG materials, including even and uneven distributions. They found that the frequencies of the beam were reduced by increasing the porosity volume fraction. Akbaş [10] presented the geometrically nonlinear analysis of FGP Timoshenko beams using the finite element method in conjunction with the Newton-Raphson method. The nonlinear vibration behavior of a S-S axially FG Euler-Bernoulli beam subjected to a moving harmonic force was examined by Alimoradzadeh et al. [11] using the Galerkin technique and the variational method. Besides analyzing the mechanical behavior of FG beams, the static and dynamic analysis of FG plates has also been reported by several authors [12-18].

* Corresponding author. Tel.: +84-946066013.
E-mail address: hieudv@tnut.edu.vn

DOI: 10.22075/macs.2021.24098.1350
Received 2021-07-30; Received in revised form 2021-10-01; Accepted 2021-12-13.

Because of the applications of micro-/nano-sized structures in micro-/nano-electromechanical systems, many scientists are interested in analyzing the mechanical behaviors of these structures. The classical elasticity theory (CET) without the length scale parameters (LSPs) is not suitable for modeling micro-/nano- sized structures. Several higher-order theories of elasticity containing the LSPs have been introduced to model the micro-/nano- sized structures, such as the nonlocal elasticity theory (NET) [19, 20] the strain gradient theory (SGT) [21-25]. To date, some versions of the SGT have been proposed, for example, the modified strain gradient theory (MSGT) [26] and the modified couple stress theory (MCST) [27]. Size-dependent behaviors of micro-/nano- sized structures can be observed in two different directions using the NET and the SGT. A stiffness softening effect can be observed by using the NET [19, 20], while a stiffness hardening effect can be observed by utilizing the SGT [21-25] and its versions [26, 27]. Some works presented the static and dynamic analysis of micro-and nano-beams reported based on these above higher-order elasticity theories [28-40]. In addition, Hou et al. [41] investigated the buckling and bending behaviors of FG micro-cylindrical imperfect beams using the MCST. Based on the MCST and EBT, the nonlinear free vibration response of the FG non-uniform micro-tube was studied by Huang et al. [42] utilizing the homotopy perturbation and the differential quadrature methods. The semi-analytical solutions for the nonlinear and linear forced vibration problems of FG non-uniform cylindrical micro-beams based on the EBT and MCST were carried out by Xu et al. [43] by applying the differential quadrature method.

Recently, both the NET and the SGT were combined in a generalized higher-order elasticity theory, the NSGT; this elasticity theory was proposed by Lim et al. [44]. The NSGT considered that the stress is a sum of the non-gradient nonlocal stress and higher-order gradient stress. In the framework of the NSGT, depending on the relationship between the NP and MLSP, the micro-/nano-sized structures arise the stiffness softening effect or stiffness hardening effect [45-49]. Many works related to the bending, stability, and vibration analysis of the FG micro-/nano-structures were reported by using the NSGT. The nonlinear vibration behavior of FG Euler-Bernoulli nano-beams was investigated by Şimşek [50], utilizing the novel Hamiltonian approach. The bending, buckling, and vibration behaviors of viscoelastic FG curved Euler-Bernoulli nano-beam resting on an elastic foundation were investigated by Allam and Radwan [51]. Nonlinear vibration behavior of an electrostatic FG Euler-Bernoulli nano-resonator taking into account the effect of surface stress was investigated by Esfahani et al. [52]. The nonlinear vibration behavior of FG nano-beams was studied by Hieu et al. [53] utilizing the NSGT considering thickness effect. The nonlinear vibration and stability characteristics of FGP Euler-Bernoulli micro-beams under electrostatic force were examined by Dang and Do [54]. Dang et al. [55] investigated the stability and nonlinear vibration behaviors of FG nano-tubes conveying fluid. The effect of magnetic field on the nonlinear vibration of electrostatically actuated FG micro-beam was reported by Hieu et al. [56]. Tang and Qing [57] studied the buckling and free vibration behaviors of the FG Timoshenko beam using the Laplace transform method. The forced vibration behavior of laminated FG graphene platelet-reinforced composite micro-beams under external harmonic forces was investigated by Wu et al. [58] using the refined hyperbolic shear deformation beam theory. Esen et al. [59] examined the dynamical behavior of FG nano-beam reinforced by carbon nanotubes subjected to a moving point load. Moreover, recently, the effects of magnetic and thermal fields on FG Timoshenko nano-beam buckling and free vibration behaviors were examined by Esen et al. [60].

The influence of porosity on the mechanical behavior of FG micro-beams is an important topic that needs to be studied. The novelty of this work is to present the analytical analysis for the buckling and nonlinear free vibration problems of the FGP micro-beam resting on the elastic foundation based on the NSGT and the EBT for the first time. The micro-beam is composed of a mixture of metal and ceramic, in which the material properties are assumed to change continuously in the direction of thickness according to the simple exponential law. Two porosity distribution models, including even and uneven distributions, are examined to consider the porosity effect. Hamilton's principle is applied to establish the governing equation of motion. The analytical expressions of the critical buckling force and nonlinear frequency of the FGP micro-beam with S-S BCs are carried out. Numerical illustrations are performed to check the accuracy and evaluate the impact of some important parameters on the nonlinear free vibration and stability behaviors of the micro-beam.

2. Model and Formulations

2.1. Modeling of the FGP Micro-beam

A model of an FGP micro-beam resting on an elastic foundation is considered in Fig. 1. The FGP micro-beam has the length *L,* width *b,* and height

h. A Winkler–Pasternak type elastic foundation with two layers is considered, including the Winkler layer with foundation coefficient kL and the Pasternak layer with foundation coefficient kS. The micro-beam is composed of metal and ceramic with porosity distribution. The material properties of the micro-beam are assumed to vary in the thickness direction according to the simple exponential law. In this work, two kinds of porosity distributions, including even and uneven distribution, are considered (see Fig. 2). The material properties, Young's modulus $E(z)$, and the mass density $\rho(z)$, can be estimated by [9]:

$$E(z) = (E_c - E_m)\left(\frac{z}{h} + \frac{1}{2}\right)^k + E_m - \frac{\delta}{2}(E_c + E_m) \quad (1)$$

$$\rho(z) = (\rho_c - \rho_m)\left(\frac{z}{h} + \frac{1}{2}\right)^k + \rho_m - \frac{\delta}{2}(\rho_c + \rho_m) \quad (2)$$

for the even porosity distribution (or FGM-I), and [9]:

$$E(z) = (E_c - E_m)\left(\frac{z}{h} + \frac{1}{2}\right)^k + E_m - \frac{\delta}{2}(E_c + E_m)\left(1 - \frac{2|z|}{h}\right) \quad (3)$$

$$\rho(z) = (\rho_c - \rho_m)\left(\frac{z}{h} + \frac{1}{2}\right)^k + \rho_m - \frac{\delta}{2}(\rho_c + \rho_m)\left(1 - \frac{2|z|}{h}\right) \quad (4)$$

For the uneven porosity distribution (FGM-II). In the above equations, subscripts "c" and "m" represent ceramic and metal phases, respectively; k $(0 \le k < \infty)$ is the power-law index which governs the change of the volume fraction of ceramic and metal phases; z is the thickness coordinate from the geometry middle surface of the FGP micro-beam, and δ $(0 \le \delta \ll 1)$ refers to the porosity distribution factor. When $\delta = 0$ (without porosity), the FGP micro-beam becomes the perfect FG micro-beam. It is noted that the perfect FG micro-beam becomes a fully ceramic micro-beam if k is equal to zero and nearly a metal micro-beam for a very large value of k.

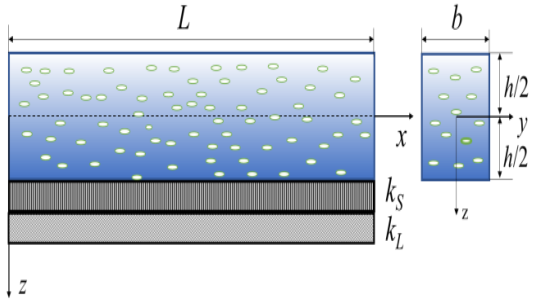

Fig. 1. Modeling of a FGP micro-beam resting on an elastic foundation

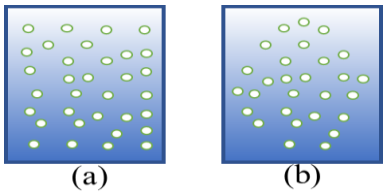

Fig. 2. Porosity distribution models: (a) even porosity distribution (FGM-I), (b) uneven porosity distribution (FGM-II)

As can see from Fig. 2, the FGM-I model has porosities uniformly distributed over the micro-beam's cross-section. At the same time, the FGM-II model has porosities spreading mostly around the middle area of the micro-beam's cross-section, and the amount of porosity decreases linearly to zero at the upper and lower surfaces of the micro-beam's cross-section.

2.2. The NSGT

The total stress of the FGP micro-beam based on the NSGT is defined as [44]:

$$t_{xx} = \sigma_{xx} - \frac{\partial \sigma_{xx}^{(1)}}{\partial x} \quad (5)$$

where $\sigma_{xx}$and $\sigma_{xx}^{(1)}$ are the nonlocal stress and the higher-order nonlocal stress, respectively, these stresses are functions of the classical strain (ε_{xx}) and the strain gradient $(\varepsilon_{xx,x})$ [44]:

$$\sigma_{xx} = \int_0^L E(z)\alpha_0(x, x', e_0 a)\varepsilon'_{xx}(x')dx' \quad (6)$$

$$\sigma_{xx}^{(1)} = l_m^2 \int_0^L E(z)\alpha_1(x, x', e_1 a)\varepsilon'_{xx,x}(x')dx' \quad (7)$$

in which, l_m is the MLSP which describes the effect of strain gradient stress field; $e_0 a$ and $e_1 a$ are the two NPs describing the effect of the nonlocal stress field; α_0 and α_1 are the two nonlocal kernel functions defined by Eringen [19, 20].

For one dimensional problem, the general nonlocal strain gradient constitutive equation takes a form [44]:

$$[1 - (e_0 a)^2\nabla^2][1 - (e_1 a)^2\nabla^2]t_{xx} = E(z)[1 - (e_1 a)^2\nabla^2]\varepsilon_{xx} - E(z)l_m^2[1 - (e_0 a)^2\nabla^2]\nabla^2\varepsilon_{xx} \quad (8)$$

where $\nabla^2 = \frac{\partial^2}{\partial x^2}$ is the Laplace operator. When considering $e_0 = e_1 = e$, Eq. (8) is reduced to:

$$[1 - (ea)^2\nabla^2]t_{xx} = [E(z) - E(z)l_m^2\nabla^2]\varepsilon_{xx} \quad (9)$$

The nonlocal constitutive equations for the NET [19, 20] and the SGT [25] can be recovered from Eq. (9) by letting $l_m = 0$ and $ea = 0$, respectively.

2.3. The Governing Equation for the FGP Micro-beam

According to the EBT and the von-Kármán's geometrical nonlinearity, the nonzero strain of the FGP micro-beam is [46, 48, 50]:

$$\varepsilon_{xx} = \frac{\partial u}{\partial x} + \frac{1}{2}\left(\frac{\partial w}{\partial x}\right)^2 - z\frac{\partial^2 w}{\partial x^2} \tag{10}$$

where u and w represent the axial and transverse displacements of any point on the geometry middle surface of the FGP micro-beam, respectively. The virtual strain energy of the FGP micro-beam based on the NSGT is given as [46, 48, 50]:

$$\delta U = \int_V \left(\sigma_{xx}\delta\varepsilon_{xx} + \sigma_{xx}^{(1)}\delta\varepsilon_{xx,x}\right) dV \tag{11}$$

Combination of Eqs. (10) and (11), leads to:

$$\begin{aligned}
\delta U = &\int_0^L \int_A \left\{ t_{xx}\delta\left[\frac{\partial u}{\partial x} + \frac{1}{2}\left(\frac{\partial w}{\partial x}\right)^2\right] \right. \\
&\left. - t_{xx} z \delta\left(\frac{\partial^2 w}{\partial x^2}\right)\right\} dA dx \\
&+ \int_A \left\{ \sigma_{xx}^{(1)}\delta\left[\frac{\partial u}{\partial x} + \frac{1}{2}\left(\frac{\partial w}{\partial x}\right)^2\right] \right. \\
&\left. - \sigma_{xx}^{(1)} z \delta\left(\frac{\partial^2 w}{\partial x^2}\right)\right\} dA \Bigg|_0^L \\
= &\int_0^L \int_A \left\{ t_{xx}\left[\frac{\partial \delta u}{\partial x} + \frac{\partial w}{\partial x}\frac{\partial \delta w}{\partial x}\right] \right. \\
&\left. - t_{xx} z \frac{\partial^2 \delta w}{\partial x^2}\right\} dA dx \\
&+ \int_A \left\{ \sigma_{xx}^{(1)}\left[\delta\left(\frac{\partial u}{\partial x}\right) + \frac{\partial w}{\partial x}\delta\left(\frac{\partial w}{\partial x}\right)\right] \right. \\
&\left. - \sigma_{xx}^{(1)} z \delta\left(\frac{\partial^2 w}{\partial x^2}\right)\right\} dA \Bigg|_0^L \\
= &\int_0^L \left\{ N_{xx}^{(1)}\left[\frac{\partial \delta u}{\partial x} + \frac{\partial w}{\partial x}\frac{\partial \delta w}{\partial x}\right] - M_{xx}^{(1)}\frac{\partial^2 \delta w}{\partial x^2}\right\} dx \\
&+ \left\{ N_{xx}^{(2)}\left[\delta\left(\frac{\partial u}{\partial x}\right) + \frac{\partial w}{\partial x}\delta\left(\frac{\partial w}{\partial x}\right)\right] \right. \\
&\left. - M_{xx}^{(2)}\delta\left(\frac{\partial^2 w}{\partial x^2}\right)\right\} \Bigg|_0^L \\
= &\left[N_{xx}^{(1)}\delta u\right]\Big|_0^L - \int_0^L \frac{\partial N_{xx}^{(1)}}{\partial x}\delta u\, dx \\
&+ \left[N_{xx}^{(1)}\frac{\partial w}{\partial x}\delta w\right]\Big|_0^L \\
&- \int_0^L \frac{\partial}{\partial x}\left[N_{xx}^{(1)}\frac{\partial w}{\partial x}\right]\delta w\, dx - \left[M_{xx}^{(1)}\delta\left(\frac{\partial w}{\partial x}\right)\right]\Big|_0^L \\
&+ \left[\frac{\partial M_{xx}^{(1)}}{\partial x}\delta w\right]\Big|_0^L - \int_0^L \frac{\partial^2 M_{xx}^{(1)}}{\partial x^2}\delta w\, dx \\
&+ \left\{ N_{xx}^{(2)}\left[\delta\left(\frac{\partial u}{\partial x}\right) + \frac{\partial w}{\partial x}\delta\left(\frac{\partial w}{\partial x}\right)\right] \right. \\
&\left. - M_{xx}^{(2)}\delta\left(\frac{\partial^2 w}{\partial x^2}\right)\right\} \Bigg|_0^L
\end{aligned} \tag{12}$$

where $N_{xx}^{(1)}$ denotes the axial force resultant, $M_{xx}^{(1)}$ denotes the bending moment resultant, $N_{xx}^{(2)}$ indicates the non-classical axial force, and $M_{xx}^{(2)}$ is the non-classical moment; these quantities are defined as:

$$\begin{aligned}
&N_{xx}^{(1)} = \int_A t_{xx} dA\,, M_{xx}^{(1)} = \int_A z t_{xx} dA, \\
&N_{xx}^{(2)} = \int_A \sigma_{xx}^{(2)} dA\,, M_{xx}^{(2)} = \int_A z\sigma_{xx}^{(2)} dA
\end{aligned} \tag{13}$$

herein, $A = b \times h$. The axial force resultant and the bending moment resultant are expressed as, respectively:

$$\begin{aligned}
&(1 - (ea)^2\nabla^2) N_{xx}^{(1)} = \\
&(1 - l_m^2\nabla^2) A_{xx}\left(\frac{\partial u}{\partial x} + \frac{1}{2}\left(\frac{\partial w}{\partial x}\right)^2\right)
\end{aligned} \tag{14}$$

$$(1 - (ea)^2\nabla^2) M_{xx}^{(1)} = -D_{xx}(1 - l_m^2\nabla^2)\frac{\partial^2 w}{\partial x^2} \tag{15}$$

where

$$A_{xx} = \int_A E(z) dA, \qquad D_{xx} = \int_A E(z) z^2 dA \tag{16}$$

The virtual kinetic energy of the FGP micro-beam is given as [48]:

$$\begin{aligned}
K_e = &\int_0^L \int_A \rho(z)\frac{\partial u_1}{\partial t}\delta\left(\frac{\partial u_1}{\partial t}\right) dA dx \\
&+ \int_0^L \int_A \rho(z)\frac{\partial u_3}{\partial t}\delta\left(\frac{\partial u_3}{\partial t}\right) dA dx \\
\approx &\int_0^L m_0\frac{\partial u}{\partial t}\delta\left(\frac{\partial u}{\partial t}\right) dx + \int_0^L m_0\frac{\partial w}{\partial t}\delta\left(\frac{\partial w}{\partial t}\right) dx \\
&+ \int_0^L m_2\frac{\partial^2 w}{\partial t \partial x}\delta\left(\frac{\partial^2 w}{\partial t \partial x}\right) dx
\end{aligned} \tag{17}$$

where:

$$m_0 = \int_A \rho(z) dA, \qquad m_2 = \int_A \rho(z) z^2 dA \tag{18}$$

The virtual external work caused by the transverse distributed force $q(x,t)$ and the elastic foundation reaction $q_e(x,t) = -k_L w + k_S\frac{\partial^2 w}{\partial x^2}$ can be calculated by:

$$\begin{aligned}
\delta W &= \int_0^L (q\delta w + q_e\delta w) dx \\
&= \int_0^L \left[q\delta w + \left(-k_L w + k_S\frac{\partial^2 w}{\partial x^2}\right)\delta w\right] dx
\end{aligned} \tag{19}$$

To get the motion equation, Hamilton's principle is employed [46-50]:

$$\int_0^t (\delta K_e - \delta U + \delta W)\, dt = 0 \tag{20}$$

Substituting Eqs. (12), (17), and (19) into Eq. (20), the following equations can be achieved:

$$\delta u: \quad \frac{\partial N_{xx}^{(1)}}{\partial x} - m_0 \frac{\partial^2 u}{\partial t^2} = 0 \tag{21}$$

$$\delta w: \quad \frac{\partial^2 M_{xx}^{(1)}}{\partial x^2} + \frac{\partial}{\partial x}\left[N_{xx}^{(1)} \frac{\partial w}{\partial x}\right] + q - k_L w + k_s \frac{\partial^2 w}{\partial x^2} - m_0 \frac{\partial^2 w}{\partial t^2} + m_2 \frac{\partial^4 w}{\partial t^2 \partial x^2} = 0 \tag{22}$$

and BCs at $x = 0$ and $x = L$:

$$\delta u: \quad N_{xx}^{(1)} = 0 \quad or \quad u = 0, \tag{23}$$

$$\delta\left(\frac{\partial u}{\partial x}\right): \quad N_{xx}^{(2)} = 0 \quad \text{or} \quad \frac{\partial u}{\partial x} = 0, \tag{24}$$

$$\delta w: \quad \frac{\partial M_{xx}^{(1)}}{\partial x} + N_{xx}^{(1)} \frac{\partial w}{\partial x} = 0 \quad \text{or} \quad w = 0, \tag{25}$$

$$\delta\left(\frac{\partial w}{\partial x}\right): \quad M_{xx}^{(1)} - N_{xx}^{(2)} \frac{\partial w}{\partial x} = 0 \quad \text{or} \quad \frac{\partial w}{\partial x} = 0, \tag{26}$$

$$\delta\left(\frac{\partial^2 w}{\partial x^2}\right): \quad M_{xx}^{(2)} = 0 \quad \text{or} \quad \frac{\partial^2 w}{\partial x^2} = 0 \tag{27}$$

From Eqs. (14), (15), (21), and (22), the expressions of the axial force and bending moment resultants can be obtained as:

$$N_{xx}^{(1)} = A_{xx}\left(1 - l_m^2 \frac{\partial^2}{\partial x^2}\right)\left[\frac{\partial u}{\partial x} + \frac{1}{2}\left(\frac{\partial w}{\partial x}\right)^2\right] + (ea)^2 m_0 \frac{\partial^3 u}{\partial x \partial t^2}, \tag{28}$$

$$M_{xx}^{(1)} = -D_{xx}\left(1 - l_m^2 \frac{\partial^2}{\partial x^2}\right)\frac{\partial^2 w}{\partial x^2} + (ea)^2 \begin{bmatrix} m_0 \frac{\partial^2 w}{\partial t^2} - m_2 \frac{\partial^4 w}{\partial t^2 \partial x^2} \\ -\frac{\partial}{\partial x}\left(N_{xx}^{(1)} \frac{\partial w}{\partial x}\right) + k_L w \\ -k_S \frac{\partial^2 w}{\partial x^2} - q \end{bmatrix} \tag{29}$$

Therefore, the equations of motion for the FGP micro-beam can be obtained by putting Eqs. (28) and (29) into Eqs. (14) and (15) as:

$$A_{xx}\frac{\partial}{\partial x}\left\{\left(1 - l_m^2 \frac{\partial^2}{\partial x^2}\right)\left[\frac{\partial u}{\partial x} + \frac{1}{2}\left(\frac{\partial w}{\partial x}\right)^2\right]\right\} - m_0 \frac{\partial^2}{\partial t^2}\left[1 - (ea)^2 \frac{\partial^2 w}{\partial x^2}\right] = 0, \tag{30}$$

$$-D_{xx}\left(1 - l_m^2 \frac{\partial^2}{\partial x^2}\right)\frac{\partial^4 w}{\partial x^4} + \frac{\partial}{\partial x}\left(N_{xx}^{(1)} \frac{\partial w}{\partial x}\right) - (ea)^2 \frac{\partial^3}{\partial x^3}\left(N_{xx}^{(1)} \frac{\partial w}{\partial x}\right) - m_0 \frac{\partial^2}{\partial t^2}\left[w - (ea)^2 \frac{\partial^2 w}{\partial x^2}\right] + m_2 \frac{\partial^4}{\partial t^2 \partial x^2}\left[w - (ea)^2 \frac{\partial^2 w}{\partial x^2}\right] - k_L\left[w - (ea)^2 \frac{\partial^2 w}{\partial x^2}\right] + k_S \frac{\partial^2}{\partial x^2}\left[w - (ea)^2 \frac{\partial^2 w}{\partial x^2}\right] + \left[q - (ea)^2 \frac{\partial^2 q}{\partial x^2}\right] = 0 \tag{31}$$

The following result can be obtained if the axial inertia terms in Eq. (30) are neglected:

$$A_{xx}\left(1 - l_m^2 \frac{\partial^2}{\partial x^2}\right)\left[\frac{\partial u}{\partial x} + \frac{1}{2}\left(\frac{\partial w}{\partial x}\right)^2\right] = C, \tag{32}$$

where C is the integral constant which can be determined by the following BCs:

$$u(L) = -\frac{P_0 L}{A_{xx}}, u(0) = \left.\frac{\partial^2 u}{\partial x_2}\right|_{x=L} = \left.\frac{\partial^2 u}{\partial x_2}\right|_{x=0} = 0, \tag{33}$$

in which, P_0 is the initial compressive axial force. Employing the BCs (33) and integrating both sides of Eq. (32) from 0 to L, it can be obtained:

$$C = -P_0 + \frac{A_{xx}}{2L}\int_0^L \left(\frac{\partial w}{\partial x}\right)^2 dx - \frac{A_{xx}}{L} l_m^2 \int_0^L \left[\frac{\partial w}{\partial x}\frac{\partial^3 w}{\partial x^3} + \left(\frac{\partial^2 w}{\partial x^2}\right)^2\right] dx. \tag{34}$$

From Eqs. (28), (32), and (34), the expression of the axial force resultant can be derived as:

$$N_{xx}^{(1)} = -P_0 + \frac{A_{xx}}{2L}\int_0^L \left(\frac{\partial w}{\partial x}\right)^2 dx - \frac{A_{xx}}{L} l_m^2 \int_0^L \left[\frac{\partial w}{\partial x}\frac{\partial^3 w}{\partial x^3} + \left(\frac{\partial^2 w}{\partial x^2}\right)^2\right] dx. \tag{35}$$

Now, substituting Eq. (35) into Eq. (31), the motion equation of the FGP micro-beam in terms of the transverse displacement (w) based on the NSGT can be derived as:

$$\left\{P_0 - \frac{A_{xx}}{2L}\int_0^L \left(\frac{\partial w}{\partial x}\right)^2 dx\right\}\left[\frac{\partial^2 w}{\partial x^2} - (ea)^2 \frac{\partial^4 w}{\partial x^4}\right] + \left\{\frac{A_{xx}}{L} l_m^2 \int_0^L \left[\frac{\partial w}{\partial x}\frac{\partial^3 w}{\partial x^3} + \left(\frac{\partial^2 w}{\partial x^2}\right)^2\right] dx\right\} \times \left[\frac{\partial^2 w}{\partial x^2} - (ea)^2 \frac{\partial^4 w}{\partial x^4}\right] + D_{xx}\left(1 - l_m^2 \frac{\partial^2}{\partial x^2}\right)\frac{\partial^4 w}{\partial x^4} + m_0 \frac{\partial^2}{\partial t^2}\left[w - (ea)^2 \frac{\partial^2 w}{\partial x^2}\right] - m_2 \frac{\partial^4}{\partial t^2 \partial x^2}\left[w - (ea)^2 \frac{\partial^2 w}{\partial x^2}\right] + k_L\left[w - (ea)^2 \frac{\partial^2 w}{\partial x^2}\right] - k_S \frac{\partial^2}{\partial x^2}\left[w - (ea)^2 \frac{\partial^2 w}{\partial x^2}\right] = \left[q - (ea)^2 \frac{\partial^2 q}{\partial x^2}\right]. \tag{36}$$

For the S-S FGP micro-beam, the classical and nonclassical BCs at $x = 0$ and $x = L$ can be expressed as [48]:

$$w = 0, \qquad \frac{\partial^2 w}{\partial x^2} = 0, \qquad \frac{\partial^4 w}{\partial x^4} = 0. \tag{37}$$

which was investigated by Şimşek [50].

Without considering the elastic foundation ($k_L = k_S = 0$) and the influence of the axial

compressive force ($P_0 = 0$), and the second mass moment of inertia are ignored ($m_2 = 0$), Eq. (36) is reduced to:

$$\begin{aligned}&\left\{-\frac{A_{xx}}{2L}\int_0^L\left(\frac{\partial w}{\partial x}\right)^2 dx\right\}\left[\frac{\partial^2 w}{\partial x^2}-(ea)^2\frac{\partial^4 w}{\partial x^4}\right]\\&+\left\{\frac{A_{xx}}{L}l_m^2\int_0^L\left[\frac{\partial w}{\partial x}\frac{\partial^3 w}{\partial x^3}+\left(\frac{\partial^2 w}{\partial x^2}\right)^2\right]dx\right\}\\&\times\left[\frac{\partial^2 w}{\partial x^2}-(ea)^2\frac{\partial^4 w}{\partial x^4}\right]+D_{xx}\left(1-l_m^2\frac{\partial^2}{\partial x^2}\right)\frac{\partial^4 w}{\partial x^4}\\&+m_0\frac{\partial^2}{\partial t^2}\left[w-(ea)^2\frac{\partial^2 w}{\partial x^2}\right]=\left[q-(ea)^2\frac{\partial^2 q}{\partial x^2}\right].\end{aligned}\tag{38}$$

For the homogeneous micro-beam, i.e.$D_{xx} = EI$, $A_{xx} = EA$, $m_0 = \rho A$ and $m_2 = \rho I$, Eq. (36) becomes:

$$\begin{aligned}&\left\{P_0-\frac{EA}{2L}\int_0^L\left(\frac{\partial w}{\partial x}\right)^2 dx\right\}\left[\frac{\partial^2 w}{\partial x^2}-(ea)^2\frac{\partial^4 w}{\partial x^4}\right]\\&+\left\{\frac{EA}{L}l_m^2\int_0^L\left[\frac{\partial w}{\partial x}\frac{\partial^3 w}{\partial x^3}+\left(\frac{\partial^2 w}{\partial x^2}\right)^2\right]dx\right\}\\&\times\left[\frac{\partial^2 w}{\partial x^2}-(ea)^2\frac{\partial^4 w}{\partial x^4}\right]+EI\left(1-l_m^2\frac{\partial^2}{\partial x^2}\right)\frac{\partial^4 w}{\partial x^4}\\&+\rho A\frac{\partial^2}{\partial t^2}\left[w-(ea)^2\frac{\partial^2 w}{\partial x^2}\right]\\&-\rho I\frac{\partial^4}{\partial t^2\partial x^2}\left[w-(ea)^2\frac{\partial^2 w}{\partial x^2}\right]\\&+k_L\left[w-(ea)^2\frac{\partial^2 w}{\partial x^2}\right]\\&-k_P\frac{\partial^2}{\partial x^2}\left[w-(ea)^2\frac{\partial^2 w}{\partial x^2}\right]=\left[q-(ea)^2\frac{\partial^2 q}{\partial x^2}\right].\end{aligned}\tag{39}$$

which was studied by Dang [46].

For the convenience of calculations, the dimensionless variables are introduced as follows:

$$\begin{aligned}&\bar{x}=\frac{x}{L},\bar{w}=\frac{w}{L},\bar{t}=t\sqrt{\frac{E_m h^2}{\rho_m L^4}},\alpha=\frac{ea}{L},\\&\beta=\frac{l_m}{L},\quad\gamma=\frac{L}{h},P=\frac{P_0L^2}{E_m bh^3},K_L=\frac{k_L L^4}{E_m bh^3},\\&K_P=\frac{k_S L^2}{E_m bh^3},\bar{q}=\frac{qL^3}{E_m bh^3},\bar{z}=\frac{z}{h},\bar{c}=\frac{c}{h}.\end{aligned}\tag{40}$$

Using Eq. (40), the motion equation of the FGP micro-beam can be rewritten in the following dimensionless form:

$$\begin{aligned}&\left\{P-\frac{\bar{A}_{xx}}{2}\gamma^2\int_0^1\left(\frac{\partial\bar{w}}{\partial\bar{x}}\right)^2 d\bar{x}\right\}\left[\frac{\partial^2\bar{w}}{\partial\bar{x}^2}-\alpha^2\frac{\partial^4\bar{w}}{\partial\bar{x}^4}\right]\\&+\left\{\bar{A}_{xx}\beta^2\gamma^2\int_0^1\left[\frac{\partial\bar{w}}{\partial\bar{x}}\frac{\partial^3\bar{w}}{\partial\bar{x}^3}+\left(\frac{\partial^2\bar{w}}{\partial\bar{x}^2}\right)^2\right]d\bar{x}\right\}\\&\times\left[\frac{\partial^2\bar{w}}{\partial\bar{x}^2}-\alpha^2\frac{\partial^4\bar{w}}{\partial\bar{x}^4}\right]+\bar{D}_{xx}\left(1-\beta^2\frac{\partial^2}{\partial\bar{x}^2}\right)\frac{\partial^4\bar{w}}{\partial\bar{x}^4}\\&+\bar{m}_0\left[\frac{\partial^2\bar{w}}{\partial\bar{t}^2}-\alpha^2\frac{\partial^4\bar{w}}{\partial\bar{t}^2\partial\bar{x}^2}\right]\\&-\bar{m}_2\frac{1}{\gamma^2}\left[\frac{\partial^4\bar{w}}{\partial\bar{t}^2\partial\bar{x}^2}-\alpha^2\frac{\partial^6\bar{w}}{\partial\bar{t}^2\partial\bar{x}^4}\right]\\&+K_L\left[\bar{w}-\alpha^2\frac{\partial^2\bar{w}}{\partial\bar{x}^2}\right]-K_S\left[\frac{\partial^2\bar{w}}{\partial\bar{x}^2}-\alpha^2\frac{\partial^4\bar{w}}{\partial\bar{x}^4}\right]\\&=\left[\bar{q}-\alpha^2\frac{\partial^2\bar{q}}{\partial\bar{x}^2}\right].\end{aligned}\tag{41}$$

Where

$$\begin{aligned}&\bar{A}_{xx}=\int_{-1/2}^{1/2}\frac{E(\bar{z})}{E_m}d\bar{z},\quad\bar{D}_{xx}=\int_{-\frac{1}{2}}^{\frac{1}{2}}\frac{E(\bar{z})}{E_m}\bar{z}^2 d\bar{z},\\&\bar{m}_0=\int_{-\frac{1}{2}}^{\frac{1}{2}}\frac{\rho(\bar{z})}{\rho_m}d\bar{z},\qquad\bar{m}_2=\int_{-1/2}^{1/2}\frac{\rho(\bar{z})}{\rho_m}\bar{z}^2 d\bar{z}\end{aligned}\tag{42}$$

Thus, the classical and nonclassical BCs at $\bar{x} = 0$and $\bar{x} = 1$ becomes:

$$\bar{w}=0,\frac{\partial^2\bar{w}}{\partial\bar{x}^2}=0,\qquad\frac{\partial^4\bar{w}}{\partial\bar{x}^4}=0\tag{43}$$

3. Solution Procedure

3.1. Buckling Analysis

For buckling analysis, ignoring the terms related to time and the transverse distributed force in Eq. (41), the equation for buckling analysis can be achieved as:

$$\begin{aligned}&\left\{P-\frac{\bar{A}_{xx}}{2}\gamma^2\int_0^1\left(\frac{\partial\bar{w}}{\partial\bar{x}}\right)^2 d\bar{x}\right\}\left[\frac{\partial^2\bar{w}}{\partial\bar{x}^2}-\alpha^2\frac{\partial^4\bar{w}}{\partial\bar{x}^4}\right]\\&+\left\{\bar{A}_{xx}\beta^2\gamma^2\int_0^1\left[\frac{\partial\bar{w}}{\partial\bar{x}}\frac{\partial^3\bar{w}}{\partial\bar{x}^3}+\left(\frac{\partial^2\bar{w}}{\partial\bar{x}^2}\right)^2\right]d\bar{x}\right\}\\&\times\left[\frac{\partial^2\bar{w}}{\partial\bar{x}^2}-\alpha^2\frac{\partial^4\bar{w}}{\partial\bar{x}^4}\right]+\bar{D}_{xx}\left(1-\beta^2\frac{\partial^2}{\partial\bar{x}^2}\right)\frac{\partial^4\bar{w}}{\partial\bar{x}^4}\\&+K_L\left[\bar{w}-\alpha^2\frac{\partial^2\bar{w}}{\partial\bar{x}^2}\right]-K_S\left[\frac{\partial^2\bar{w}}{\partial\bar{x}^2}-\alpha^2\frac{\partial^4\bar{w}}{\partial\bar{x}^4}\right]=0.\end{aligned}\tag{44}$$

With S-S BCs, the solution of Eq. (44) can be assumed as:

$$\bar{w}=\sum_{n=1}^{\infty}W_n\sin(n\pi\bar{x})\tag{45}$$

where n denotes the number of half-waves, substituting the solution (45) into Eq. (44), leads to:

$$\bar{W}_n^2 = -\frac{4\bar{D}_{xx}c_2}{\bar{A}_{xx}\gamma^2 c_1} + \frac{4P}{\bar{A}_{xx}\gamma^2\lambda^2} - \frac{4K_L}{\bar{A}_{xx}\gamma^2\lambda^4} - \frac{4K_S}{\bar{A}_{xx}\gamma^2\lambda^2} \tag{46}$$

in which

$$c_1 = 1 + \alpha^2\lambda^2; c_2 = 1 + \beta^2\lambda^2, \lambda = n\pi \tag{47}$$

By letting $\bar{W}_n = 0$ in Eq. (46), the dimensionless critical buckling force can be achieved as:

$$P_{cr} = \frac{\bar{D}_{xx}\lambda^2 c_2}{c_1} + \frac{K_L}{\lambda^2} + K_S \tag{48}$$

Considering Eqs. (40) and (42), the physical form of the critical buckling force can be achieved as:

$$(P_0)_{cr} = \frac{D_{xx}\lambda^2 c_2}{L^2 c_1} + \frac{k_L}{\lambda^2} + k_S = \frac{D_{xx}(n\pi)^2(1+\beta^2 n^2\pi^2)}{L^2(1+\alpha^2 n^2\pi^2)} + \frac{k_L}{(n\pi)^2} + k_S \tag{49}$$

For the homogeneous micro-beam and without the elastic foundation, the critical buckling force becomes:

$$(P_0)_{cr} = \frac{EI(n\pi)^2(1+\beta^2 n^2\pi^2)}{L^2(1+\alpha^2 n^2\pi^2)} \tag{50}$$

which is the same as a result achieved by Li and Hu [47]. For the classical homogeneous micro-beam, the critical buckling force (50) reduces to:

$$(P_0)_{cr} = \frac{EI(n\pi)^2}{L^2} \tag{51}$$

It can be observed that the dimensionless MLSP (β) increases the critical buckling force, while the dimensionless NP (α) decreases the critical buckling force. The elastic foundation coefficients lead to an increase in the critical buckling force.

3.2. Nonlinear Vibration Analysis

For free nonlinear vibration analysis, letting $P = 0$ and $\bar{q}_0$, Eq. (41) becomes:

$$\begin{aligned}
&\left\{-\frac{\bar{A}_{xx}}{2}\gamma^2\int_0^1\left(\frac{\partial\bar{w}}{\partial\bar{x}}\right)^2 d\bar{x}\right\}\left[\frac{\partial^2\bar{w}}{\partial\bar{x}^2} - \alpha^2\frac{\partial^4\bar{w}}{\partial\bar{x}^4}\right] \\
&+\left\{\bar{A}_{xx}\beta^2\gamma^2\int_0^1\left[\frac{\partial\bar{w}}{\partial\bar{x}}\frac{\partial^3\bar{w}}{\partial\bar{x}^3} + \left(\frac{\partial^2\bar{w}}{\partial\bar{x}^2}\right)^2\right]d\bar{x}\right\} \\
&\times\left[\frac{\partial^2\bar{w}}{\partial\bar{x}^2} - \alpha^2\frac{\partial^4\bar{w}}{\partial\bar{x}^4}\right] + \bar{D}_{xx}\left(1-\beta^2\frac{\partial^2}{\partial\bar{x}^2}\right)\frac{\partial^4\bar{w}}{\partial\bar{x}^4} \\
&+\bar{m}_0\left[\frac{\partial^2\bar{w}}{\partial\bar{t}^2} - \alpha^2\frac{\partial^4\bar{w}}{\partial\bar{t}^2\partial\bar{x}^2}\right] \\
&-\bar{m}_2\frac{1}{\gamma^2}\left[\frac{\partial^4\bar{w}}{\partial\bar{t}^2\partial\bar{x}^2} - \alpha^2\frac{\partial^6\bar{w}}{\partial\bar{t}^2\partial\bar{x}^4}\right] \\
&+K_L\left[\bar{w} - \alpha^2\frac{\partial^2\bar{w}}{\partial\bar{x}^2}\right] - K_S\left[\frac{\partial^2\bar{w}}{\partial\bar{x}^2} - \alpha^2\frac{\partial^4\bar{w}}{\partial\bar{x}^4}\right] = 0.
\end{aligned} \tag{52}$$

which is the nonlinear partial differential equation (PDE); the exact solution of this equation is very difficult to find. Therefore, the approximate solution is an effective choice. First, the Galerkin technique will be applied to convert the nonlinear PDE (52) into the nonlinear ordinary differential equation (ODE). To apply the Galerkin technique, the solution of the nonlinear PDE (52) is assumed to have the form:

$$\bar{w}(\bar{x},\bar{t}) = Q(\bar{t})\phi(\bar{x}) \tag{53}$$

where, the time-dependent function $Q(\bar{t})$ needs to be found, the shape function $\phi(\bar{x})$ is chosen so that the solution (53) satisfies the BCs (43). For the S-S FGP micro-beam, the shape function can be chosen as follows [46, 50]:

$$\phi(\bar{x}) = sin\,\pi\,\bar{x} \tag{54}$$

Now, applying the Galerkin technique to the nonlinear PDE (52), the following nonlinear ODE can be obtained:

$$\ddot{Q}(\bar{t}) + \gamma_1 Q(\bar{t}) + \gamma_2 Q^3(\bar{t}) = 0 \tag{55}$$

where:

$$\gamma_1 = \frac{\begin{bmatrix}\bar{D}_{xx}\int_0^1\phi^{(4)}\phi d\bar{x} - \beta^2\bar{D}_{xx}\int_0^1\phi^{(6)}\phi d\bar{x} \\ +K_L\left(\int_0^1\phi^2 d\bar{x} - \alpha^2\int_0^1\phi''\phi d\bar{x}\right) \\ -K_S\left(\int_0^1\phi''\phi d\bar{x} - \alpha^2\int_0^1\phi^{(4)}\phi d\bar{x}\right)\end{bmatrix}}{\begin{bmatrix}\bar{m}_0\left(\int_0^1\phi^2 d\bar{x} - \alpha^2\int_0^1\phi''\phi d\bar{x}\right) \\ -\frac{\bar{m}_2}{\gamma^2}\left(\int_0^1\phi''\phi d\bar{x} - \alpha^2\int_0^1\phi^{(4)}\phi d\bar{x}\right)\end{bmatrix}} \tag{56}$$

$$\gamma_2 = \frac{\left\{\bar{A}_{xx}\gamma^2\begin{bmatrix}-\frac{1}{2}\int_0^1(\phi')^2 d\bar{x} \\ +\beta^2\int_0^1\phi'\phi^{(3)}d\bar{x} \\ +\beta^2\int_0^1(\phi'')^2 d\bar{x}\end{bmatrix}\begin{pmatrix}\int_0^1\phi''\phi d\bar{x} \\ -\alpha^2\int_0^1\phi^{(4)}\phi d\bar{x}\end{pmatrix}\right\}}{\begin{bmatrix}\bar{m}_0\left(\int_0^1\phi^2 d\bar{x} - \alpha^2\int_0^1\phi''\phi d\bar{x}\right) \\ -\frac{\bar{m}_2}{\gamma^2}\left(\int_0^1\phi''\phi d\bar{x} - \alpha^2\int_0^1\phi^{(4)}\phi d\bar{x}\right)\end{bmatrix}} \tag{57}$$

Eq. (55) is the nonlinear ODE which is assumed to satisfy the following initial conditions:

$$Q(0) = Q_0, \dot{Q}(0) = 0 \tag{58}$$

where $Q_0 = \bar{w}_{max}$ is the dimensionless vibrational amplitude of the FGP micro-beam.

It can see that Eq. (55) is the cubic-Duffing nonlinear oscillator which can be solved by many different analytical methods [61]. In this section, the ELM and a weighted averaging value [62-64] will be used to find the approximate analytical solution of Eq. (55). According to the ELM, the replacement of nonlinear equation (55) by a linear equation is performed, in which the weighted averaging value is employed to estimate the coefficients of the linear equation. Accordingly, the amplitude-frequency relationship of the FGP micro-beam can be achieved as:

$$\omega_{NL} = \sqrt{\gamma_1 + 0.72\gamma_2 Q_0^2} \tag{59}$$

Using the shape function in Eq. (54), the integrals in Eqs. (56) and (57) can be calculated as:

$$\begin{aligned}
&\int_0^1 \phi^2 d\bar{x} = \frac{1}{2}; \int_0^1 \phi''\phi d\bar{x} = -\frac{\pi^2}{2};\\
&\int_0^1 (\phi')^2 d\bar{x} = \frac{\pi^2}{2}; \int_0^1 (\phi'')^2 d\bar{x} = \frac{\pi^4}{2};\\
&\int_0^1 \phi'\phi^{(3)} d\bar{x} = -\frac{\pi^4}{2}; \int_0^1 \phi^{(4)}\phi d\bar{x} = \frac{\pi^4}{2};\\
&\int_0^1 \phi^{(6)}\phi d\bar{x} = -\frac{\pi^6}{2}.
\end{aligned} \tag{60}$$

Substituting the results in Eq. (60) into Eqs. (56) and (58); and then replacing the obtained results into Eq. (59), the expression of nonlinear frequency of the FGP micro-beam can be achieved as follows:

$$\omega_{NL} = \sqrt{\begin{bmatrix} \dfrac{\bar{D}_{xx}\pi^4(1+\pi^2\beta^2)}{(1+\pi^2\alpha^2)\left(\bar{m}_0 + \dfrac{\bar{m}_2\pi^2}{\gamma^2}\right)} \\ + \dfrac{K_L}{\left(\bar{m}_0 + \dfrac{\bar{m}_2\pi^2}{\gamma^2}\right)} + \dfrac{K_S\pi^2}{\left(\bar{m}_0 + \dfrac{\bar{m}_2\pi^2}{\gamma^2}\right)} \end{bmatrix} + 0.72\left[\dfrac{\bar{A}_{xx}\pi^4\gamma^2}{4\left(\bar{m}_0 + \dfrac{\bar{m}_2\pi^2}{\gamma^2}\right)}\right] Q_0^2} \tag{61}$$

The linear frequency of the FGP micro-beam can be obtained from the nonlinear frequency (61) by letting Q_0 as:

$$\omega_L = \sqrt{\begin{bmatrix} \dfrac{\bar{D}_{xx}\pi^4(1+\pi^2\beta^2)}{(1+\pi^2\alpha^2)\left(\bar{m}_0 + \dfrac{\bar{m}_2\pi^2}{\gamma^2}\right)} \\ + \dfrac{K_L}{\left(\bar{m}_0 + \dfrac{\bar{m}_2\pi^2}{\gamma^2}\right)} + \dfrac{K_S\pi^2}{\left(\bar{m}_0 + \dfrac{\bar{m}_2\pi^2}{\gamma^2}\right)} \end{bmatrix}} \tag{62}$$

The elastic foundation coefficients (and) lead to an increase in the FGP micro-beam frequencies. The FGP micro-beam frequencies increase by increasing the dimensionless MLSP (β) or decreasing the value of the dimensionless NP (α).

4. Numerical Results

To verify the accuracy of present results and predict the buckling and free vibration behaviors of the FGP micro-beam, a micro-beam composed of Aluminum (Al-metal) and Alumina (Alumina Al_2O_3-ceramic) is considered. Table 1 shows the material properties of Al and Al_2O_3.

For the classical perfect FG beam, the present results are compared with those obtained by Thai and Vo [5]. The comparison is shown in Table 2. A very good agreement between the obtained linear frequency and the one achieved by Thai and Vo [5] can be observed in Table 2.

Table 1 The material properties of Al and Al_2O_3

Materials	E (GPa)	ρ (kg/m^3)
Al	$E_m = 70$	$\rho_m = 2702$
Al_2O_3	$E_c = 380$	$\rho_c = 3960$

Table 2 The dimensionless linear frequencies of the FG beam

k	L/h=5		L/h=20	
	Ref. [5]	Present	Ref. [5]	Present
0	5.3953	5.3953	5.4777	5.4777
0.5	4.5931	4.5932	4.6641	4.6641
1	4.1484	4.1485	4.2163	4.2163
2	3.7793	3.7796	3.8472	3.8472
5	3.5949	3.5952	3.6628	3.6628
10	3.4921	3.4923	3.5547	3.5547

4.1. Buckling

To study the buckling response of the FGP micro-beam, the critical buckling force ratio (R_{cr}) and the scale ratio (χ) are defined as follows:

$$R_{cr} = \frac{P_{cr}}{(P_{cr})_{classical}}, \chi = \frac{\alpha}{\beta} = \frac{ea}{l_m} \tag{63}$$

where $(P_{cr})_{classical}$ is the dimensionless classical critical buckling force of the full metal micro-beam.

The effects of the dimensionless MLSP β and the dimensionless NP α on the critical buckling force ratio R_{cr} of the FGP micro-beam are presented in Fig. 3. It can be seen that the classical results ($\chi = 0$ and $\alpha = 0$) are equal to the NSG results if $\chi = 1$. If $\chi < 1$ (i.e.,$\alpha < \beta$), the critical buckling force ratio increases as the dimensionless MLSP increases. The critical buckling force ratio decreases as the dimensionless MLSP increases if $\chi > 1$ (i.e., $\alpha > \beta$). The obtained result is suited to the result obtained by Dang [46], Li, and Hu [47]. Employing the NSGT, the FGP micro-beam exert the softening and hardening effects corresponding to $\chi > 1$ and $\chi < 1$, respectively.

The effect of the power-law index k on the buckling behavior of the FGP micro-beam is presented in Fig. 4. It can be observed that k has the effect of decreasing the value of P_{cr}. The FGP micro-beam will be more flexible as k increases; this leads to a decrease P_{cr}. As can see from this figure, the critical buckling forces of the FGM-II micro-beam are always larger than those of the FGM-I micro-beam. This result can be explained as follows: with porosities distributed mainly in the middle surface of the micro-beam's cross-section and the amount of porosity seeming to decrease linearly to zero at the upper and lower surfaces of the micro-beam's cross-section, the FGM-II micro-beam have a greater stiffness than the FGM-I micro-beam.

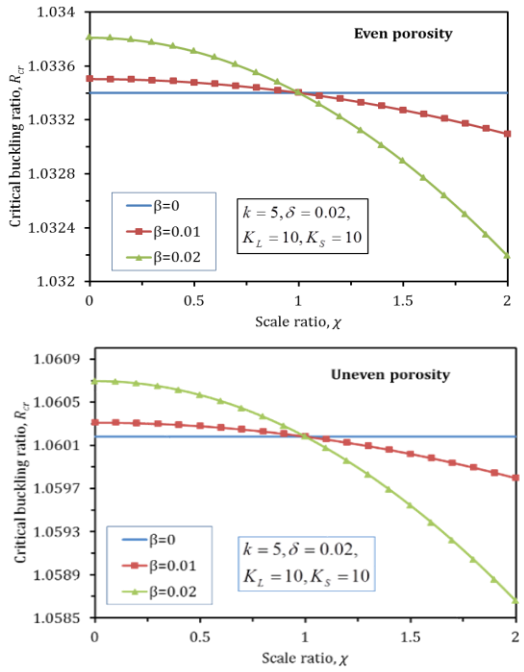

Fig. 3. The variation of R_{cr} to χ for some values of β

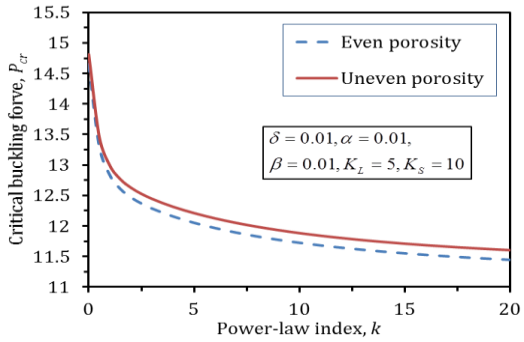

Fig. 4. Variation of P_{cr} to k with $\delta = 0.01, \alpha = 0.01$, $\beta = 0.01, K_L = 5$ and $K_S = 10$.

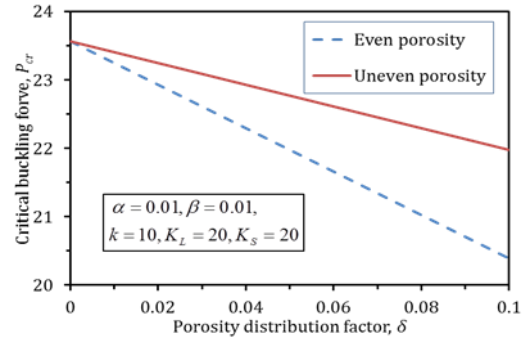

Fig. 5. Variation of P_{cr} to δ

Fig. 5 reveals the influence of the porosity distribution factor δ on the variation of the dimensionless critical buckling force P_{cr}. The critical buckling force P_{cr} decreases linearly when the porosity distribution factor δ increases. The fact the stiffness of FGP micro-beams reduces by increasing the porosity distribution factor, and thus, the critical buckling force decreases. The critical buckling forces of the FGM-I micro-beam are always smaller than those of the FGM-II micro-beam (it is the same as Fig. 4).

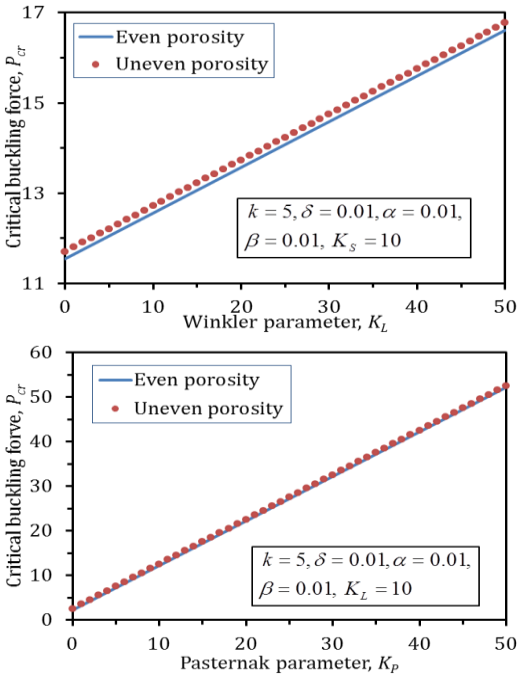

Fig. 6. Variation of P_{cr} to K_L (a) and K_S (b)

The effects of the elastic foundation coefficients on the variation of the critical buckling force of the FGP micro-beam can be seen in Fig. 6. The coefficients of the elastic foundation lead to an increase in the value P_{cr}. This result is completely consistent because the elastic foundation enhances the stiffness of the FGP micro-beam.

4.2. Nonlinear Vibration

To observe the effects of the dimensionless MLSP and NP on the nonlinear free vibration behavior of the FGP micro-beam, Fig. 7 shows the variation of the nonlinear frequency ω_{NL} to the scale ratio $\chi = ea/l_m$ for some values of the dimensionless MLSP β. The nonlinear frequencies of the FGP classical micro-beams (i. e.,$\alpha = \beta = 0$) are equal to those of the FGP NSG micro-beams if $\chi = 1$ (namely,$\alpha = \beta$). It can also be observed that the scale ratio χ leads to a decrease of the value of ω_{NL}. It is a fact that ω_{NL} decreases when the dimensionless NP increases due to the softening effect observed in the NET. If $\chi < 1$ (namely, $\alpha < \beta$), the dimensionless MLSP has the effect of increasing the value of ω_{NL}. This means that the MLSP makes the hardening effect as in the SGT. If $\chi > 1$ (namely, $\alpha > \beta$), the MLSP has the effect of decreasing the value of ω_{NL}; again, the softening effect can be observed.

The effect of the power-law index k on the variation of ω_{NL} can be observed in Fig. 8. It can be seen that k has an interesting impact on the vibration behavior of the FGP micro-beam. This figure indicates that ω_{NL} increases strongly with small values of k ($k \leq 5$) and decreases slowly with larger values of k.

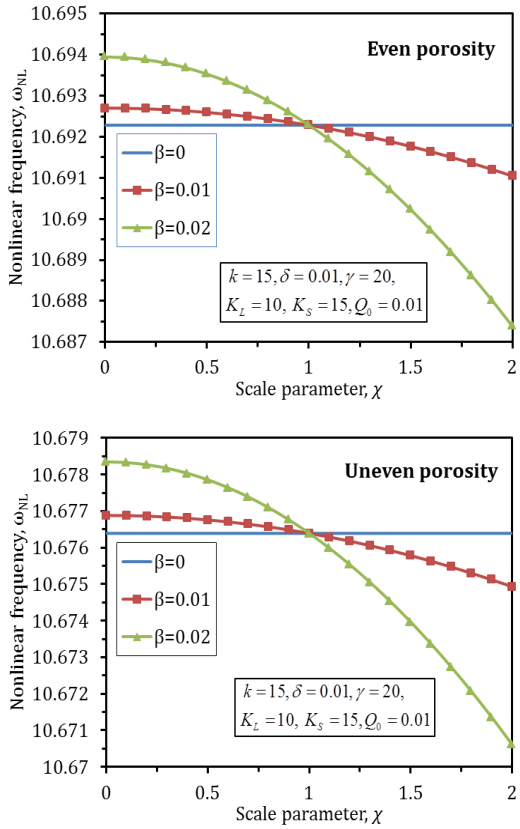

Fig. 7. Variation of ω_{NL} to χ for some values β

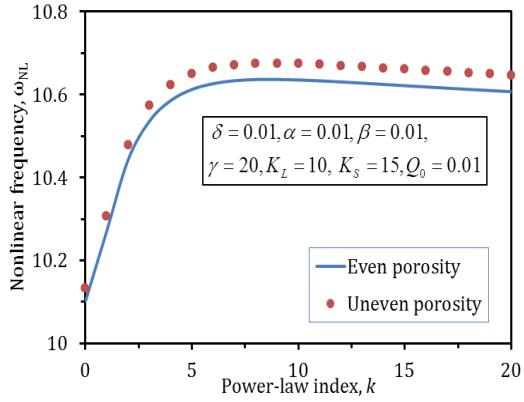

Fig. 8. Variation of ω_{NL} to k

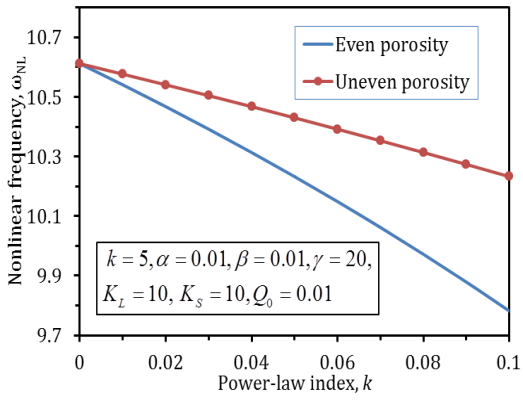

Fig. 9. Variation of the nonlinear frequency ω_{NL} to the porosity distribution factor δ

Fig. 9 shows the effect of δ on the variation of ω_{NL} of the FGP micro-beam. It can be concluded that ω_{NL} decreases when δ increases. When the value of δ increases from 0.04 to 0.08, the nonlinear frequency reduces about 1.52% for FGM-II microbeams and 3.28% for FGM-I microbeams. The nonlinear frequencies of the FGM-II micro-beams are always larger than those of the FGM-I micro-beams. This result can be explained as the stiffness of the FGM-II microbeam is larger than that of the FGM-I microbeam. This result completely agrees with the results obtained by Wattanasakulpong and Chaikittiratana [9], Dang and Do [54].

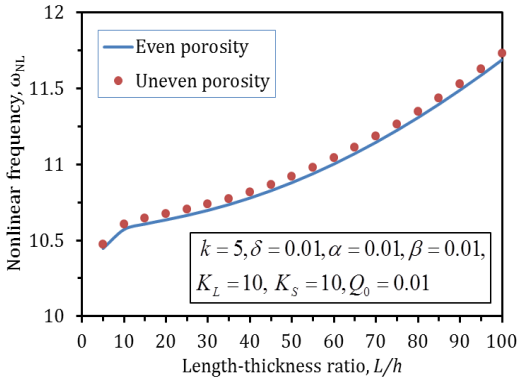

Fig. 10. Variation of the nonlinear frequency ω_{NL} to the length-thickness ratio L/h

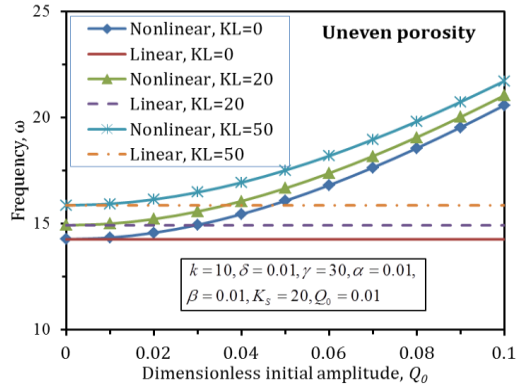

Fig. 11. Variation of frequencies ω to Q_0 for some values of K_L

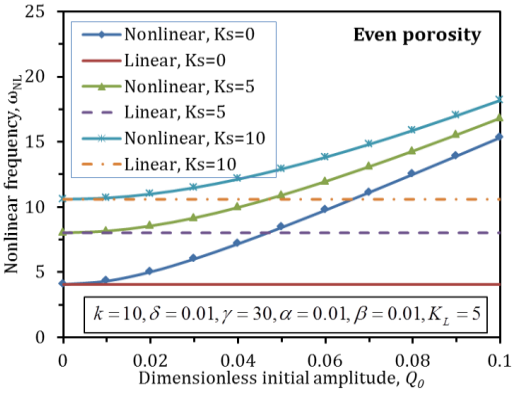

Fig. 12. Variation of frequencies ω to Q_0 for some values of K_S

The effect of the length-thickness ratio L/h on the variation of ω_{NL} is shown in Fig. 10. From this figure, it can be concluded that ω_{NL}increase when the length-thickness ratio increases. This result is consistent with those obtained by Thai and Vo [5], Dang [46].

Figures 11 and 12 show the variations of the frequencies (ω) of the FGP micro-beam to the dimensionless Winkler parameter K_L and the dimensionless Pasternak parameter K_S, respectively. The elastic foundation makes the FGP micro-beam stiffer, so the frequencies of the FGP micro-beam increase as the coefficients of the elastic foundation increase. Also, these figures increase when the dimensionless initial amplitude increases. When considering the effect of geometrical nonlinearity, the micro-beam's frequency increases rapidly as the initial amplitude increases.

5. Conclusion

The EBT is developed based on the NSGT to investigate the buckling and nonlinear free vibration problems of the imperfect FG micro-beam with porosities resting on an elastic foundation. The analytical expressions of the critical buckling force and the nonlinear frequency of the S-S FGP micro-beam are obtained using the Galerkin technique and the ELM. Numerical illustrations are performed, through which the accuracy of the results is verified, and the impact of some important parameters on the micro-beam's behavior is evaluated. Some points can be concluded as follows:

- An increase of the power-law index k leads to a reduction of the critical buckling force, while k has an interesting effect on the variation of the nonlinear frequency of the micro-beam.
- When$ea < l_m$, the MLSP leads to an increase of both the critical buckling force and the nonlinear frequency. Moreover, on the other hand when $ea > l_m$, the MLSP reduces the critical buckling force and the nonlinear frequency.
- The length-thickness ratio leads to an increase in the value of the nonlinear frequency.
- The elastic foundation makes the FGP micro-beam stiffer, and consequently, both the critical buckling force and the nonlinear frequency increase as increasing the coefficients of the elastic foundation.

Acknowledgments

This research is supported by the Thai Nguyen University of Technology (TNUT).

References

[1] Koizumi, M., 1993. Concept of FGM. *Ceramic Transactions*, *34*, pp. 3-10.

[2] Koizumi, M., 1997. FGM activities in Japan. *Composites Part B: Engineering*, *28* (1-2), pp.1-4.

[3] Jha, D.K., Kant, T., & Singh, R.K., 2013. A critical review of recent research on functionally graded plates. *Composite Structures*, *96*, pp. 833–849.

[4] Fallah, A., Aghdam, M.M., 2011. Nonlinear free vibration and post-buckling analysis of functionally graded beams on nonlinear elastic foundation. *European Journal of Mechanics A/Solids*, *30*, pp. 571-583.

[5] Thai, H.T. & Vo, T.P., 2012. Bending and free vibration of functionally graded beams using various higher-order shear deformation beam theories. *International Journal of Mechanical Sciences*, *62*, pp. 57–66.

[6] Yan, T., Yang, T. & Chen, L., 2020. Direct Multiscale Analysis of Stability of an Axially Moving Functionally Graded Beam with Time-Dependent Velocity. *Acta Mechanica Solida Sinica*, *33*, pp. 150–163.

[7] Jahwari, F.A, Anwer, A.A., Naguib, H.E., 2015. Fabrication and microstructural characterization of functionally graded porous acrylonitrile butadiene styrene and the effect of cellular morphology on creep behavior. *Journal of Polymer Science Part B: Polymer Physics*, *53*, pp. 795–803.

[8] Jahwari, F.A., Huang, Y., Naguib, H.E., Lo, J., 2016. Relation of impact strength to the microstructure of functionally graded porous structures of acrylonitrile butadiene styrene (ABS) foamed by thermally activated microspheres. *Polymer*, *98*, pp. 270–281.

[9] Wattanasakulpong, N. & Chaikittiratana, A., 2015. Flexural vibration of imperfect functionally graded beams based on Timoshenko beam theory: Chebyshev collocation method. *Meccanica*, *50*, pp. 1331–1342.

[10] Akbaş, Ş.D., 2018. Geometrically nonlinear analysis of functionally graded porous beams. *Wind & Structures*, *27*(1), pp. 59-70.

[11] Alimoradzadeh, M., Salehi, M., & Esfarjani, S.M., 2019. Nonlinear Dynamic Response of an Axially Functionally Graded (AFG) Beam Resting on Nonlinear Elastic Foundation Subjected to Moving Load. *Nonlinear Engineering*, *8*, pp. 250–260

[12] Uymaz, B. & Aydogdu, M., 2013. Three dimensional mechanical buckling of FG plates with general boundary conditions. *Composite Structures*, *96*, pp. 174-193.

[13] Rouzegar, J. & Abad, F., 2015. Free vibration analysis of FG plate with piezoelectric layers

using four-variable refined plate theory. *Thin-Walled Structures*, *89*, pp. 76-83.

[14] Wu, C.P. & Yu, L.T., 2019. Free vibration analysis of bi-directional functionally graded annular plates using finite annular prism methods. *Journal of Mechanical Science and Technology*, *33*, pp. 2267–2279.

[15] Tornabene, F., Viola, E. & Inman, D.J., 2009. 2-D differential quadrature solution for vibration analysis of functionally graded conical, cylindrical shell and annular plate structures. *Journal of Sound and Vibration*, *328(3)*, pp. 259–290.

[16] Xue, Y., Li, J., Li, F. et al., 2020. Flutter and Thermal Buckling Properties and Active Control of Functionally Graded Piezoelectric Material Plate in Supersonic Airflow. *Acta Mechanica Solida Sinica*, *33*, pp. 692–706.

[17] Civalek, Ö., 2020. Vibration of functionally graded carbon nanotube reinforced quadrilateral plates using geometric transformation discrete singular convolution method. *International Journal for Numerical Methods in Engineering*, *121(5)*, pp. 990-1019.

[18] Kiani, Y. (2016). Free vibration of FG-CNT reinforced composite skew plates. Aerospace Science and Technology, *58*, 178-188.

[19] Eringen, A.C. & Edelen, D.G.B., 1972. On nonlocal elasticity. *International Journal of Engineering Science*, *10*, pp. 233-248.

[20] Eringen, A.C., 1983. On differential equations of nonlocal elasticity and solutions of screw dislocation and surface waves. *Journal of Applied Physics*, *54*, pp. 4703-10.

[21] Mindlin, R.D. & Tiersten, H.F., 1962. Effects of couple-stresses in linear elasticity. *Archive for Rational Mechanics and Analysis*, *11(1)*, pp. 415–448.

[22] Mindlin, R.D., 1964. Micro-structure in linear elasticity. Archive for Rational Mechanics and Analysis, *16(1)*, pp. 51–78.

[23] Mindlin, R.D., 1965. Second gradient of strain and surface-tension in linear elasticity. *International Journal of Solids and Structures*, *1(1)*, pp. 417–438.

[24] Toupin, R.A., 1962. Elastic materials with couple-stresses. *Archive for Rational Mechanics and Analysis*, *11(1)*, pp. 385–414.

[25] Aifantis, E.C., 1992. On the role of gradients in the localization of deformation and fracture. *International Journal of Engineering Science*, *30(10)*, pp. 1279–1299.

[26] Yang, F., Chong, A.C.M., Lam, D.C.C., et al., 2002. Couple stress based strain gradient theory for elasticity. *International Journal of Solids and Structures*, *39(10)*, pp. 2731–2743.

[27] Lam, D.C.C., Yang, F., Chong, A.C.M., et al., 2003. Experiments and theory in strain gradient elasticity. *Journal of Mechanics and Physics of Solids*, *51(8)*, pp. 1477–1508.

[28] Thai, H.T., 2012. A nonlocal beam theory for bending, buckling, and vibration of nano-beams. *International Journal of Engineering Science*, *52*, pp. 56–64.

[29] Eltaher, M.A., Khater, M.E. & Emam, S.A., 2016. A review on nonlocal elastic models for bending, buckling, vibrations, and wave propagation of nanoscale beams. *Applied Mathematical Modelling*, *40(5-6)*, pp. 4109–4128.

[30] Reddy, J.N., 2007. Nonlocal theories for bending, buckling and vibration of beams. *International Journal of Engineering Science*, *45*, pp. 288–307.

[31] Reddy, J.N. & Pang, S.D., 2008. Nonlocal continuum theories of beams for the analysis of carbon nanotubes. *Journal of Applied Physics*, *103(2)*, 023511.

[32] Kong, S.L., Zhou, S.J., Nie, Z.F. & Wang, K., 2008. Static and dynamic analysis of micro beams based on strain gradient elasticity theory. *International Journal of Engineering Science*, *47*, pp. 487–498.

[33] Akgöz, B. & Civalek, Ö., 2013. A size-dependent shear deformation beam model based on the strain gradient elasticity theory. *International Journal of Engineering Science*, *70*, pp. 1–14.

[34] Roque, C.M.C., Fidalgo, D.S., Ferreira, A.J.M. & Reddy, J.N., 2013. A study of a microstructure dependent composite laminated Timoshenko beam using a modified couple stress theory and a meshless method. *Composite Structures*, *96*, pp. 532-537.

[35] Chen, W., Weiwei, C. & Sze, K.Y. (2012). A model of composite laminated Reddy beam based on a modified couple-stress theory. Composite Structures, *94*, 2599–609.

[36] Ghayes, M.H., Amabili, M. & Farokhi, H., 2013. Nonlinear forced vibrations of a microbeam based on the strain gradient elasticity theory. *International Journal of Engineering Science*, *63*, pp. 52–60.

[37] Dang, V., Nguyen, D., Le, M. et al., 2020. Nonlinear vibration of microbeams based on the nonlinear elastic foundation using the equivalent linearization method with a weighted averaging. *Archive of Applied Mechanics*, *90*, pp. 87–106.

[38] Akbaş, Ş.D., 2018. Forced vibration analysis of cracked nano-beams. *Journal of the Brazilian Society of Mechanical Sciences and Engineering*, *40(8)*, pp. 1-11.

[39] Akbaş, Ş.D., 2018. Bending of a cracked functionally graded nano-beam. *Advances in Nano Research, 6(3)*, pp. 219-242.

[40] Kocaturk, T., & Akbaş, Ş.D., 2013. Wave propagation in a microbeam based on the modified couple stress theory. *Structural engineering and mechanics: An international journal*, *46(3)*, pp. 417-431.

[41] Hou, F., Wu, S., Moradi, Z. and Shafiei, N., 2021. The computational modeling for the static analysis of axially functionally graded micro-cylindrical imperfect beam applying the computer simulation. *Engineering with Computers*, pp.1-19.

[42] Huang, X., Zhang, Y., Moradi, Z. and Shafiei, N., 2021. Computer simulation via a couple of homotopy perturbation methods and the generalized differential quadrature method for nonlinear vibration of functionally graded non-uniform micro-tube. *Engineering with Computers*, pp.1-18.

[43] Xu, W., Pana, G., Moradi, Z., & Shafiei, N., 2021. Nonlinear forced vibration analysis of functionally graded non-uniform cylindrical microbeams applying the semi-analytical solution. *Composite Structures, 275*, pp. 1-15.

[44] Lim, C.W., Zhang, G., & Reddy, J.N., 2015. A higher-order nonlocal elasticity and strain gradient theory and its applications in wave propagation. *Journal of the Mechanics and Physics of Solids*, *78*, pp. 298–313.

[45] Dang, V., Nguyen, D., Le, M. et al., 2020. Nonlinear vibration of nano-beams under electrostatic force based on the nonlocal strain gradient theory. *International Journal of Mechanics and Materials in Design*, *16*, pp. 289–308.

[46] Dang, V.H., 2020. Buckling and Nonlinear Vibration of Size-Dependent Nanobeam based on the Non-Local Strain Gradient Theory. *Journal of Applied Nonlinear Dynamics*, *9(3)*, pp. 427-446.

[47] Li, L. & Hu, Y., 2015. Buckling analysis of size-dependent nonlinear beams based on a nonlocal strain gradient theory. *International Journal of Engineering Science*, *97*, pp. 84–94.

[48] Li, L. & Hu, Y., 2016. Nonlinear bending and free vibration analyses of nonlocal strain gradient beams made of functionally graded material. *International Journal of Engineering Science, 107*, pp. 77–97.

[49] Lu, L., Guo, X. & Zhao, J., 2017. Size-dependent vibration analysis of nano-beams based on the nonlocal strain gradient theory. *International Journal of Engineering Science*, *116*, pp. 12–24.

[50] Şimşek, M., 2016. Nonlinear free vibration of a functionally graded nano-beam using nonlocal strain gradient theory and a novel Hamiltonian approach. *International Journal of Engineering Science*, *105*, pp. 12–27.

[51] Allam, M.N.M. & Radwan, A.F., 2019. Nonlocal strain gradient theory for bending, buckling, and vibration of viscoelastic functionally graded curved nano-beam embedded in an elastic medium. *Advances in Mechanical Engineering*, *11(4)*, pp. 1–15.

[52] Esfahani, S., Khadem, S.E. & Mamaghani, A.E., 2019. Nonlinear Vibration Analysis of an Electrostatic Functionally Graded Nano-Resonator with Surface Effects Based on Nonlocal Strain Gradient Theory. *International Journal of Mechanical Sciences*, *151*, pp. 508-522.

[53] Hieu, D.V., Duong, T.H. & Bui, G.P., 2020. Nonlinear Vibration of a Functionally Graded Nanobeam Based on the Nonlocal Strain Gradient Theory considering Thickness Effect. *Advances in Civil Engineering*, *2020*.

[54] Dang, V.H. & Do, Q.C., 2021. Nonlinear vibration and stability of functionally graded porous microbeam under electrostatic actuation. *Archive of Applied Mechanics*, *91*, pp. 2301–2329.

[55] Dang, V.H., Sedighi, H.M., Chan, D.Q., Civalek, Ö. & Abouelregal, A.E., 2021. Nonlinear vibration and stability of FG nanotubes conveying fluid via nonlocal strain gradient theory. *Structural Engineering and Mechanics*, *78(1)*, pp. 103-116.

[56] Hieu, D.V., Hoa, N.T., Duy, L.Q. & Thoa, N.T.K., 2021. Nonlinear Vibration of an Electrostatically Actuated Functionally Graded Microbeam under Longitudinal Magnetic Field. *Journal of Applied and Computational Mechanics*, *7(3)*, pp. 1537-1549.

[57] Tang, Y. & Qing, H., 2021. Elastic buckling and free vibration analysis of functionally graded Timoshenko beam with nonlocal strain gradient integral model. *Applied Mathematical Modelling*, *96*, pp. 657-677

[58] Wu, Q., Chen, H. & Gao, W., 2020. Nonlocal strain gradient forced vibrations of FG-GPLRC nanocomposite microbeams. *Engineering with Computers*, *36*, pp. 1739–1750.

[59] Esen, I., Daikh, A.A. & Eltaher, M.A., 2021. Dynamic response of nonlocal strain gradient FG nano-beam reinforced by carbon nanotubes under moving point load. *The European Physical Journal Plus*, *136* (4), 458.

[60] Esen, I., Abdelrhmaan, A.A. and Eltaher, M.A., 2021. Free vibration and buckling stability of FG nanobeams exposed to magnetic and thermal fields. *Engineering with Computers*, pp.1-20.

[61] Bayat, M., Pakar, I. & Domairry, G., 2012. Recent developments of some asymptotic methods and their applications for nonlinear

vibration equations in engineering problems: a review. *Latin American Journal of Solids Structures*, *9(2)*, pp. 145-234.

[62] Anh, N.D., Hai, N.Q. & Hieu, D.V., 2017. The equivalent linearization method with a weighted averaging for analyzing of nonlinear vibrating systems. *Latin American Journal of Solids Structures*, *14(9)*, pp. 1723-1740.

[63] Hieu, D.V., Hai, N.Q. & Hung, D.T., 2018. The Equivalent Linearization Method with a Weighted Averaging for Solving Undamped Nonlinear Oscillators. *Journal of Applied Mathematics, 2018*, pp. 1-15.

[64] Hieu, D.V., 2019. A New Approximate Solution for a Generalized Nonlinear Oscillator. *International Journal of Applied and Computational Mathematics*, *5(5)*, pp. 1-13.